Progress In Electromagnetics Research, PIER 48, 1–25, 2004

PROPAGATORS AND SCATTERING OF ELECTROMAGNETIC WAVES IN PLANAR BIANISOTROPIC SLABS — AN APPLICATION TO FREQUENCY SELECTIVE STRUCTURES

G. Kristensson

Department of Electroscience
Lund Institute of Technology
P.O. Box 118, SE-221 00 Lund, Sweden

S. Poulsen

Chelton Applied Composites AB
Garvaren, SE-341 60 Ljungby, Sweden

S. Rikte

Kockums AB, SE-205 55 Malmö, Sweden

Abstract—Scattering by planar geometries with plane metal inclusions are analysed. The metal inclusions can be of arbitrary shape, and the material of the supporting slabs can be any linear (bianisotropic) material. We employ the method of propagators to find the solution of the scattering problem. The method has certain similarities with a vector generalisation of the transmission line theory. A general relation between the electric fields and the surface current densities on the metal inclusions and the exciting fields is found. Special attention is paid to the case of a periodic metal pattern (frequency selective structures, FSS). The method is illustrated by a series of numerical computations.

1. INTRODUCTION

Wave propagation in planar geometries is a classical canonical scattering and radiation problem and many excellent papers and books treat this problem in great detail, see *e.g.*, [2, 7, 12, 17]. Any attempt to revisit this problem have to focus on a new systematic approach to solve the problem. This is exactly the reason and motivation of this paper. The concept of propagators that relates the total transverse fields to each other provides such a new concept. Moreover, it provides a systematic approach to analyse the solution of complicated scattering problems. The use of propagators in science is old, *e.g.*, in quantum mechanics [1], but seems to have been of little use in electromagnetic problems.

The work presented in this paper grew out of the analysis presented in [9] where an integral representation technique was applied. We present a novel approach — based on the concept of propagators — to solve scattering problems in planar geometries with an arbitrary number of metallic sheets imbedded in a slab. The method has certain similarities with a vector generalisation of the transmission line theory [3, 14]. Specifically, the propagator technique is a vector

generalisation of the voltage-current transmission theory formulation [3] or transmission (ABCD) matrix [14].

The material in the supporting slabs can be arbitrary linear material, *i.e.*, a bianisotropic material [12]. The integral representation approach presented in [9] can be generalised to treat also the more general case presented in this paper, but with an increasing complexity in the analysis. The proposed method with propagators makes considerable simplification in the analysis.

An important application of the theory presented in this paper is the case when the metallic scatterers are arranged in a periodic pattern. This is the frequency selective surface or structure case (FSS) and the theory and analysis of this application is thoroughly given in [13]. In the latter part of this paper the FSS geometry is analysed and the advantages with the propagator approach become more transparent. The importance of dielectric layers in the design of a frequency selective surface is thoroughly treated in the excellent book of Munk [13].

The paper is organised in the following way: In Sections 2 and 3 the geometry and the prerequisites of the problem are presented. The propagators and the concept of wave splitting are presented in Section 4, and the general solution to the propagation problem is given in Section 5. We specialise the analysis to the periodic case in Section 6 and give some numerical examples of the analysis in Section 7. The paper ends with conclusions in Section 8.

2. GEOMETRY

The geometry of the problem analysed in this paper is depicted in Figure 1. The depth parameter z is defined by the common normal of the indicated parallel interfaces. There are N thin, plane, metallic, perfectly conducting, scatterers (patches or apertures), $S_1, S_2, \ldots, S_N$, present, each of which is supported by a bianisotropic slab, *i.e.*, there are $N+1$ slabs, occupying the region $V_1, V_2, \ldots, V_{N+1}$. The locations of the thin scatterers are $z = z_n,\ n = 1, 2, \ldots, N$. The ends of the structure are represented by the coordinates z_0 and z_{N+1}. Thus, the location of the interfaces and the thin scatterers satisfies

$$z_0 \leq z_1 < z_2 < \cdots < z_{N-1} < z_N \leq z_{N+1}$$

We recall the time-harmonic ($e^{-i\omega t}$) constitutive relations of the general bianisotropic medium [15]:

$$\begin{cases} \boldsymbol{D} = \epsilon_0\{\boldsymbol{\epsilon} \cdot \boldsymbol{E} + \eta_0 \boldsymbol{\xi} \cdot \boldsymbol{H}\} \\ \boldsymbol{B} = \dfrac{1}{c_0}\{\boldsymbol{\zeta} \cdot \boldsymbol{E} + \eta_0 \boldsymbol{\mu} \cdot \boldsymbol{H}\} \end{cases}$$

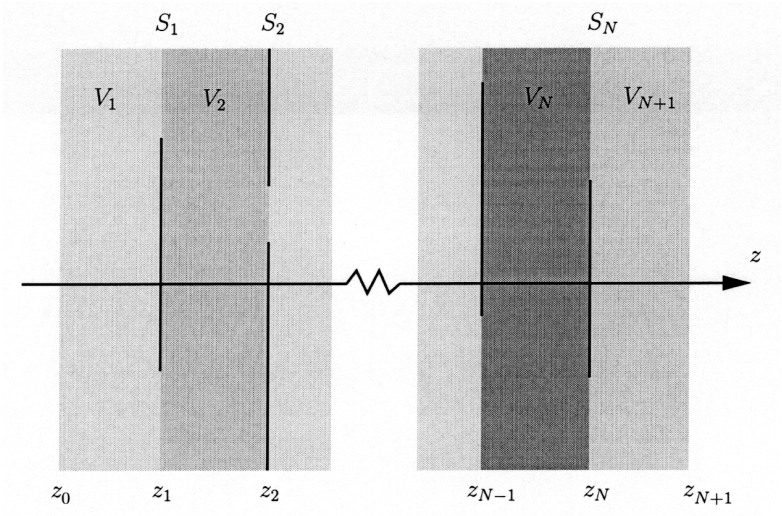

Figure 1. The geometry of the problem with patches or apertures at $z = z_1, \ldots, z_N$.

The permittivity and permeability of vacuum are denoted by ϵ_0 and μ_0, respectively. The speed of light in vacuum is $c_0 = 1/\sqrt{\epsilon_0\mu_0}$ and the intrinsic impedance of vacuum is $\eta_0 = \sqrt{\mu_0/\epsilon_0}$. The bianisotropic slabs may have varying material dyadics $\boldsymbol{\epsilon}$, $\boldsymbol{\xi}$, $\boldsymbol{\zeta}$, $\boldsymbol{\mu}$, as functions of depth z (and angular frequency ω), *i.e.*, $\boldsymbol{\epsilon} = \boldsymbol{\epsilon}(z)$ etc. In particular, they can be homogeneous or stratified. In the lateral directions, x- and y-directions, there are no variations in the material parameters. The dynamics of the fields in the bianisotropic medium is modelled by the time-harmonic Maxwell equations in a source-free region:

$$\begin{cases} \nabla \times \boldsymbol{E} = ik_0c_0\boldsymbol{B} = ik_0\{\boldsymbol{\zeta} \cdot E + \eta_0\boldsymbol{\mu} \cdot \boldsymbol{H}\} \\ \eta_0\nabla \times \boldsymbol{H} = -ik_0c_0\eta_0\boldsymbol{D} = -ik_0\{\boldsymbol{\epsilon} \cdot \boldsymbol{E} + \eta_0\boldsymbol{\xi} \cdot \boldsymbol{H}\} \end{cases} \tag{1}$$

where $k_0 = \omega/c_0$ is the vacuum wave number. The space outside the slabs is assumed to be vacuous, which covers all situation of interest in technical applications. The case of non-vacuous half spaces can be obtained as a limit process $z_0 \to -\infty$ and $z_{N+1} \to \infty$.

The sources of the problem are assumed to be confined to the regions (may be at infinity) located to the left or the right of all inhomogeneities, *i.e.*, they are contained in the vacuous half-spaces $z < z_0$ and $z > z_{N+1}$.

3. LATERAL FOURIER TRANSFORM OF THE FIELDS

With the geometry adopted in this paper, it is natural to decompose the fields in a spectrum of plane waves. The Fourier transform $\boldsymbol{E}(\boldsymbol{k}_t, z)$ of a time-harmonic field $\boldsymbol{E}(\boldsymbol{r})$, $\boldsymbol{r} = \hat{\boldsymbol{x}}x + \hat{\boldsymbol{y}}y + \hat{\boldsymbol{z}}z$, with respect to the lateral position vector $\boldsymbol{\rho} = \hat{\boldsymbol{x}}x + \hat{\boldsymbol{y}}y$ is defined by

$$\boldsymbol{E}(\boldsymbol{k}_t, z) = \iint_{-\infty}^{\infty} \boldsymbol{E}(\boldsymbol{r}) e^{-i\boldsymbol{k}_t \cdot \boldsymbol{\rho}} dx\, dy$$

where the real vector

$$\boldsymbol{k}_t = \hat{\boldsymbol{x}}k_x + \hat{\boldsymbol{y}}k_y$$

is the lateral wave vector and the non-negative (real) number

$$k_t = \sqrt{k_x^2 + k_y^2}$$

is the lateral wave number. By the Fourier inversion formula,

$$\boldsymbol{E}(\boldsymbol{r}) = \frac{1}{4\pi^2} \iint_{-\infty}^{\infty} \boldsymbol{E}(\boldsymbol{k}_t, z) e^{i\boldsymbol{k}_t \cdot \boldsymbol{\rho}} dk_x\, dk_y \tag{2}$$

Observe that only the argument of the field indicates whether the field itself $\boldsymbol{E}(\boldsymbol{r})$ or its Fourier transform $\boldsymbol{E}(\boldsymbol{k}_t, z)$ w.r.t. $\boldsymbol{\rho}$ is intended, and that the (real) unit vectors

$$\begin{cases} \hat{\boldsymbol{e}}_{\parallel}(\boldsymbol{k}_t) = \boldsymbol{k}_t / k_t \\ \hat{\boldsymbol{e}}_{\perp}(\boldsymbol{k}_t) = \hat{\boldsymbol{z}} \times \hat{\boldsymbol{e}}_{\parallel}(\boldsymbol{k}_t) \end{cases}$$

constitute a orthogonal basis for the lateral vectors (vectors in the x-y-plane).

3.1. Consequences for the Maxwell Equations

As a consequence of lateral Fourier transformation of the electric and magnetic fields, the Maxwell equations (1) for the bianisotropic medium are transformed into the system of six coupled ordinary differential equations (ODE)

$$\begin{cases} \dfrac{d}{dz}\mathbf{J} \cdot \boldsymbol{E}(\boldsymbol{k}_t, z) + i\boldsymbol{k}_t \times \boldsymbol{E}(\boldsymbol{k}_t, z) = ik_0(\boldsymbol{\zeta}(z) \cdot \boldsymbol{E}(\boldsymbol{k}_t, z) + \boldsymbol{\mu}(z) \cdot \eta_0 \boldsymbol{H}(\boldsymbol{k}_t, z)) \\ \dfrac{d}{dz}\mathbf{J} \cdot \eta_0 \boldsymbol{H}(\boldsymbol{k}_t, z) + i\boldsymbol{k}_t \times \eta_0 \boldsymbol{H}(\boldsymbol{k}_t, z) = -ik_0(\boldsymbol{\epsilon}(z) \cdot \boldsymbol{E}(\boldsymbol{k}_t, z) + \boldsymbol{\xi}(z) \cdot \eta_0 \boldsymbol{H}(\boldsymbol{k}_t, z)) \end{cases}$$

where the dyadic $\mathbf{J} = \hat{\boldsymbol{z}} \times \mathbf{I}_2$ represents a projection in the x-y-plane and a rotation of $\pi/2$ around the z-axis. One has $\mathbf{J} = \hat{\boldsymbol{e}}_\perp \hat{\boldsymbol{e}}_\parallel - \hat{\boldsymbol{e}}_\parallel \hat{\boldsymbol{e}}_\perp$.

By utilising the unique decomposition of the fields in their lateral components, $\boldsymbol{E}_{xy}(\boldsymbol{k}_t, z)$ and $\eta_0 \boldsymbol{H}_{xy}(\boldsymbol{k}_t, z)$, and their corresponding longitudinal (z) components, $E_z(\boldsymbol{k}_t, z)$ and $\eta_0 H_z(\boldsymbol{k}_t, z)$, *i.e.*,

$$\begin{cases} \boldsymbol{E}(\boldsymbol{k}_t, z) = \boldsymbol{E}_{xy}(\boldsymbol{k}_t, z) + \hat{\boldsymbol{z}} E_z(\boldsymbol{k}_t, z) \\ \boldsymbol{H}(\boldsymbol{k}_t, z) = \boldsymbol{H}_{xy}(\boldsymbol{k}_t, z) + \hat{\boldsymbol{z}} H_z(\boldsymbol{k}_t, z) \end{cases}$$

and by introducing these decompositions in the Maxwell equations, it follows that the longitudinal field components can be eliminated. A system of ODE:s for the lateral fields, the fundamental equation for one-dimensional time-harmonic wave propagation in bianisotropic materials [15], remains:

$$\frac{d}{dz} \begin{pmatrix} \boldsymbol{E}_{xy}(\boldsymbol{k}_t, z) \\ \mathbf{J} \cdot \eta_0 \boldsymbol{H}_{xy}(\boldsymbol{k}_t, z) \end{pmatrix} = ik_0 \mathbf{M}(\boldsymbol{k}_t, z) \cdot \begin{pmatrix} \boldsymbol{E}_{xy}(\boldsymbol{k}_t, z) \\ \mathbf{J} \cdot \eta_0 \boldsymbol{H}_{xy}(\boldsymbol{k}_t, z) \end{pmatrix} \tag{3}$$

where the linear map $\mathbf{M}(\boldsymbol{k}_t, z) : \mathbb{C}^2 \times \mathbb{C}^2 \to \mathbb{C}^2 \times \mathbb{C}^2$ depends on the material dyadics. A detailed representation of $\mathbf{M}(\boldsymbol{k}_t, z)$ in terms of $\boldsymbol{\epsilon}(z)$, $\boldsymbol{\xi}(z)$, $\boldsymbol{\zeta}(z)$, $\boldsymbol{\mu}(z)$, $\boldsymbol{k}_t$, and k_0 is given in [15]. In homogeneous regions, the map $\mathbf{M}(\boldsymbol{k}_t, z)$ is independent of z, *i.e.*, $\mathbf{M}(\boldsymbol{k}_t, z) = \mathbf{M}(\boldsymbol{k}_t)$. Specifically, in vacuum, $\mathbf{M}(\boldsymbol{k}_t)$ is given by

$$\mathbf{M}_0(\boldsymbol{k}_t) = \begin{pmatrix} \mathbf{0} & -\mathbf{I}_2 + \frac{1}{k_0^2} \boldsymbol{k}_t \boldsymbol{k}_t \\ -\mathbf{I}_2 - \frac{1}{k_0^2} \boldsymbol{k}_t \times (\boldsymbol{k}_t \times \mathbf{I}_2) & \mathbf{0} \end{pmatrix} \tag{4}$$

where the identity dyadic in $\mathbb{R}^2$ for lateral vectors $\mathbf{I}_2 = \hat{\boldsymbol{e}}_\parallel \hat{\boldsymbol{e}}_\parallel + \hat{\boldsymbol{e}}_\perp \hat{\boldsymbol{e}}_\perp$ introduced.

The eigenvalues of the vacuum quantity $k_0 \mathbf{M}_0(\boldsymbol{k}_t)$ defined in (4) are found to be k_z, k_z, $-k_z$, and $-k_z$, where the longitudinal wave number k_z is

$$k_z = \left(k_0^2 - k_t^2\right)^{1/2} = \begin{cases} \sqrt{k_0^2 - k_t^2} & \text{for } k_t < k_0 \\ i\sqrt{k_t^2 - k_0^2} & \text{for } k_t > k_0 \end{cases} \tag{5}$$

and the standard convention of the square root of a non-negative argument is intended. Consequently, k_z is a real non-negative number for propagating waves and a purely imaginary number with non-negative imaginary part for evanescent waves. Thus, for plane waves in vacuum regions, the general solution is of the form

$$\begin{cases} \boldsymbol{E}(\boldsymbol{k}_t, z) = \boldsymbol{E}^+(\boldsymbol{k}_t) e^{ik_z z} + \boldsymbol{E}^-(\boldsymbol{k}_t) e^{-ik_z z} \\ \boldsymbol{H}(\boldsymbol{k}_t, z) = \boldsymbol{H}^+(\boldsymbol{k}_t) e^{ik_z z} + \boldsymbol{H}^-(\boldsymbol{k}_t) e^{-ik_z z} \end{cases} \tag{6}$$

where $\boldsymbol{E}^{\pm}(\boldsymbol{k}_t)$ and $\boldsymbol{H}^{\pm}(\boldsymbol{k}_t)$ are constant, complex vectors.

4. PROPAGATION IN THE STRATIFIED REGION

The wave propagator concept for the total Fourier transformed lateral electromagnetic field proved almost indispensable in [15]. The propagator maps the Fourier transformed lateral fields at z to another position z'. Formally we write

$$\begin{pmatrix} \boldsymbol{E}_{xy}(\boldsymbol{k}_t, z) \\ \eta_0 \mathbf{J} \cdot \boldsymbol{H}_{xy}(\boldsymbol{k}_t, z) \end{pmatrix} = \mathbf{P}(\boldsymbol{k}_t, z, z') \cdot \begin{pmatrix} \boldsymbol{E}_{xy}(\boldsymbol{k}_t, z') \\ \eta_0 \mathbf{J} \cdot \boldsymbol{H}_{xy}(\boldsymbol{k}_t, z') \end{pmatrix} \tag{7}$$

This formulation is a vector generalisation of the voltage-current transmission theory formulation [3] or transmission (ABCD) matrix [14]. The propagator satisfy the same system of ODE:s as the lateral fields (3), *i.e.*,

$$\begin{cases} \dfrac{d}{dz}\mathbf{P}(\boldsymbol{k}_t, z, z') = ik_0 \mathbf{M}(\boldsymbol{k}_t, z) \cdot \mathbf{P}(\boldsymbol{k}_t, z, z') \\ \mathbf{P}(\boldsymbol{k}_t, z', z') = \mathbf{I}_4 \end{cases}$$

The augmented initial condition when both z-arguments of the propagator $\mathbf{P}$ coincide is due to the fact that the lateral fields at z then are mapped onto themselves, *i.e.*, the identity mapping $\mathbf{I}_4$ in $\mathbb{C}^4$.

Several examples of explicit expressions of the propagators are found in [15]. Specifically, the propagator for vacuum is [15]

$$\begin{aligned} \mathbf{P}_0(\boldsymbol{k}_t, z, z') &= e^{ik_0(z-z')\mathbf{M}_0(\boldsymbol{k}_t)} \\ &= \mathbf{I}_4 \cos k_z(z-z') + \frac{ik_0}{k_z}\mathbf{M}_0(\boldsymbol{k}_t) \sin k_z(z-z') \end{aligned} \tag{8}$$

where the longitudinal wave number k_z is given by (5).

4.1. Wave Splitting

We introduce a wave-splitting technique that decomposes any Fourier transformed field into two components that transport power in the $+z$- or the $-z$-directions, respectively. An alternative characterisation of the wave splitting transformation is that this transformation projects out the incident and reflected (transmitted) fields out of the total field. The wave-splitting technique in vacuum is presented in detail in *e.g.*, [15]. We have

$$\begin{pmatrix} \boldsymbol{E}_{xy}(\boldsymbol{k}_t, z) \\ \eta_0 \mathbf{J} \cdot \boldsymbol{H}_{xy}(\boldsymbol{k}_t, z) \end{pmatrix} = \begin{pmatrix} \mathbf{I}_2 & \mathbf{I}_2 \\ -\mathbf{W}^{-1}(\boldsymbol{k}_t) & \mathbf{W}^{-1}(\boldsymbol{k}_t) \end{pmatrix} \cdot \begin{pmatrix} \boldsymbol{F}^{+}(\boldsymbol{k}_t, z) \\ \boldsymbol{F}^{-}(\boldsymbol{k}_t, z) \end{pmatrix} \tag{9}$$

where[†]

$$\mathbf{W}^{-1}(\boldsymbol{k}_t) = \frac{k_0}{k_z}\left(\mathbf{I}_0 + \frac{1}{k_0^2}\boldsymbol{k}_t \times (\boldsymbol{k}_t \times \mathbf{I}_2)\right) = \hat{\boldsymbol{e}}_\parallel \hat{\boldsymbol{e}}_\parallel \frac{k_0}{k_z} + \hat{\boldsymbol{e}}_\perp \hat{\boldsymbol{e}}_\perp \frac{k_z}{k_0}$$

where, as above, $\mathbf{I}_2$ is the identity dyadic in the x-y-plane. The inverse of this dyadic in the x-y-plane is

$$\mathbf{W}(\boldsymbol{k}_t) = \frac{k_z}{k_0}\left(\mathbf{I}_0 - \frac{1}{k_z^2}\boldsymbol{k}_t \times (\boldsymbol{k}_t \times \mathbf{I}_2)\right) = \hat{\boldsymbol{e}}_\parallel \hat{\boldsymbol{e}}_\parallel \frac{k_z}{k_0} + \hat{\boldsymbol{e}}_\perp \hat{\boldsymbol{e}}_\perp \frac{k_0}{k_z}$$

and we have

$$\begin{pmatrix} \boldsymbol{F}^+(\boldsymbol{k}_t, z) \\ \boldsymbol{F}^-(\boldsymbol{k}_t, z) \end{pmatrix} = \frac{1}{2}\begin{pmatrix} \mathbf{I}_2 & -\mathbf{W}(\boldsymbol{k}_t) \\ \mathbf{I}_2 & \mathbf{W}(\boldsymbol{k}_t) \end{pmatrix} \cdot \begin{pmatrix} \boldsymbol{E}_{xy}(\boldsymbol{k}_t, z) \\ \eta_0 \mathbf{J} \cdot \boldsymbol{H}_{xy}(\boldsymbol{k}_t, z) \end{pmatrix} \tag{10}$$

To see the physical implications of this transformation, we proceed by finding the PDE for the split fields $\boldsymbol{F}^\pm$ in vacuum. The transverse fields $\boldsymbol{E}_{xy}(\boldsymbol{k}_t, z)$ and $\boldsymbol{H}_{xy}(\boldsymbol{k}_t, z)$ satisfy, see (3) and (4)

$$\frac{d}{dz}\begin{pmatrix} \boldsymbol{E}_{xy}(\boldsymbol{k}_t, z) \\ \mathbf{J} \cdot \eta_0 \boldsymbol{H}_{xy}(\boldsymbol{k}_t, z) \end{pmatrix} = ik_z \begin{pmatrix} \mathbf{0} & -\mathbf{W}(\boldsymbol{k}_t) \\ -\mathbf{W}^{-1}(\boldsymbol{k}_t) & \mathbf{0} \end{pmatrix} \cdot \begin{pmatrix} \boldsymbol{E}_{xy}(\boldsymbol{k}_t, z) \\ \mathbf{J} \cdot \eta_0 \boldsymbol{H}_{xy}(\boldsymbol{k}_t, z) \end{pmatrix}$$

since

$$\begin{cases} \mathbf{I}_2 - \dfrac{1}{k_0^2}\boldsymbol{k}_t\boldsymbol{k}_t = \dfrac{k_z}{k_0}\mathbf{W}(\boldsymbol{k}_t) \\ \mathbf{I}_2 + \dfrac{1}{k_0^2}\boldsymbol{k}_t \times (\boldsymbol{k}_t \times \mathbf{I}_2) = \dfrac{k_z}{k_0}\mathbf{W}^{-1}(\boldsymbol{k}_t) \end{cases}$$

An application of (9) and (10) gives

$$\frac{d}{dz}\begin{pmatrix} \boldsymbol{F}^+(\boldsymbol{k}_t, z) \\ \boldsymbol{F}^-(\boldsymbol{k}_t, z) \end{pmatrix} = ik_z \begin{pmatrix} \mathbf{I}_2 & \mathbf{0} \\ \mathbf{0} & -\mathbf{I}_2 \end{pmatrix} \cdot \begin{pmatrix} \boldsymbol{F}^+(\boldsymbol{k}_t, z) \\ \boldsymbol{F}^-(\boldsymbol{k}_t, z) \end{pmatrix}$$

From this equation we see that the split fields $\boldsymbol{F}^\pm$ decouple in vacuum and the solution is

$$\boldsymbol{F}^\pm(\boldsymbol{k}_t, z) = \boldsymbol{F}^\pm(\boldsymbol{k}_t, z_0) e^{\pm ik_z(z - z_0)}$$

[†] This dyadic is related to the admittance dyadic $\boldsymbol{Y}(\boldsymbol{k}_t)$.

$$\boldsymbol{Y}(\boldsymbol{k}_t) = \frac{1}{k_0 k_z}\left\{k_0^2 \hat{\boldsymbol{e}}_\perp \hat{\boldsymbol{e}}_\parallel - k_z^2 \hat{\boldsymbol{e}}_\parallel \hat{\boldsymbol{e}}_\perp\right\} = \mathbf{J} \cdot \mathbf{W}^{-1}(\boldsymbol{k}_t)$$

4.2. Propagators

The notion of propagator, defined in (7), is a very powerful tool for the analysis of wave propagation for a geometry as depicted Figure 1. In each of the bianisotropic regions we have ($n = 0, \ldots, N$)

$$\begin{pmatrix} \boldsymbol{E}_{xy}(\boldsymbol{k}_t, z_n^+) \\ \eta_0 \mathbf{J} \cdot \boldsymbol{H}_{xy}(\boldsymbol{k}_t, z_n^+) \end{pmatrix} = \mathbf{P}(\boldsymbol{k}_t, z_n, z_{n+1}) \cdot \begin{pmatrix} \boldsymbol{E}_{xy}(\boldsymbol{k}_t, z_{n+1}^-) \\ \eta_0 \mathbf{J} \cdot \boldsymbol{H}_{xy}(\boldsymbol{k}_t, z_{n+1}^-) \end{pmatrix} \tag{11}$$

where the wave propagator

$$\mathbf{P}(\boldsymbol{k}_t, z_n, z_{n+1}) = \begin{pmatrix} \mathbf{P}_{ee}(\boldsymbol{k}_t, z_n, z_{n+1}) & \mathbf{P}_{em}(\boldsymbol{k}_t, z_n, z_{n+1}) \\ \mathbf{P}_{me}(\boldsymbol{k}_t, z_n, z_{n+1}) & \mathbf{P}_{mm}(\boldsymbol{k}_t, z_n, z_{n+1}) \end{pmatrix}$$

for the general linear medium was presented in [15]. Similarly, for the two vacuous half spaces

$$\begin{pmatrix} \boldsymbol{E}_{xy}(\boldsymbol{k}_t, z) \\ \eta_0 \mathbf{J} \cdot \boldsymbol{H}_{xy}(\boldsymbol{k}_t, z) \end{pmatrix} = \mathbf{P}(\boldsymbol{k}_t, z, z_0) \cdot \begin{pmatrix} \boldsymbol{E}_{xy}(\boldsymbol{k}_t, z_0) \\ \eta_0 \mathbf{J} \cdot \boldsymbol{H}_{xy}(\boldsymbol{k}_t, z_0) \end{pmatrix}, \quad z < z_0 \tag{12}$$

$$\begin{pmatrix} \boldsymbol{E}_{xy}(\boldsymbol{k}_t, z) \\ \eta_0 \mathbf{J} \cdot \boldsymbol{H}_{xy}(\boldsymbol{k}_t, z) \end{pmatrix} = \mathbf{P}(\boldsymbol{k}_t, z, z_{N+1}) \cdot \begin{pmatrix} \boldsymbol{E}_{xy}(\boldsymbol{k}_t, z_{N+1}) \\ \eta_0 \mathbf{J} \cdot \boldsymbol{H}_{xy}(\boldsymbol{k}_t, z_{N+1}) \end{pmatrix}, \quad z > z_{N+1} \tag{13}$$

where the propagators are given explicitly by (8).

In the following section these relations between the transverse fields at different z-coordinates are exploited more in detail, and their use to solve the wave propagation problem becomes clear.

5. GENERAL FORMULATION OF PROBLEM

We are now in a position of combining the results of the previous sections together. The main concepts in the context are the notion of propagators, *i.e.*, the equations in Section 4 (8), and the wave splitting concept presented in Section 4 (7). The latter concept makes the necessary decomposition of the fields outside the slabs in order to identify the correct input and output components of the field.

Since the longitudinal components of the fields have been eliminated, and only the transverse components remain, the boundary conditions imply that the field quantities, $\boldsymbol{E}_{xy}(\boldsymbol{k}_t, z)$ and $\eta_0 \boldsymbol{H}_{xy}(\boldsymbol{k}_t, z)$, are continuous in z over any non-metallic interface. Moreover, at the thin, metallic sheets the electric field $\boldsymbol{E}_{xy}(\boldsymbol{k}_t, z_n)$ is continuous in z,

since it is zero from both sides at the metallic parts, *i.e.*, zero at z_n^+ and at z_n^- and continuous in z everywhere outside the metallic parts. However, the magnetic field $\boldsymbol{H}_{xy}(\boldsymbol{k}_t, z_n)$ has a jump discontinuity in z due to the presence of the induced surface currents on the metal parts. The total induced current distributions (sum from both sides) on the N different screens are

$$\boldsymbol{J}_S(\boldsymbol{k}_t, z_n) = \mathbf{J} \cdot \boldsymbol{H}_{xy}(\boldsymbol{k}_t, z_n^+) - \mathbf{J} \cdot \boldsymbol{H}_{xy}(\boldsymbol{k}_t, z_n^-),\ n = 1, \ldots, N \quad (14)$$

where, as above, the dyadic $\mathbf{J} = \hat{\boldsymbol{z}} \times \mathbf{I}_2$.

Equation (11) is now used to relate the fields at different z-positions. We apply (11) directly to the the internal slabs, *i.e.*, for $n = 1, \ldots, N-1$. The exterior slabs, *i.e.*, for $n = 0$ and $n = N$, is next to a half space, and to identify the correct input and output parts of the fields, we first apply the wave splitting transformation, (10). This is necessary in order to identify the pertinent reflection and transmission quantities of the entire slab and its metal scatterer. The result of the wave splitting transformation is

$$\begin{pmatrix} \boldsymbol{F}^+(\boldsymbol{k}_t, z_0) \\ \boldsymbol{F}^-(\boldsymbol{k}_t, z_0) \end{pmatrix} = \frac{1}{2} \begin{pmatrix} \mathbf{P}_{ee} - \mathbf{W} \cdot \mathbf{P}_{me} & \mathbf{P}_{em} - \mathbf{W} \cdot \mathbf{P}_{mm} \\ \mathbf{P}_{ee} + \mathbf{W} \cdot \mathbf{P}_{me} & \mathbf{P}_{em} + \mathbf{W} \cdot \mathbf{P}_{mm} \end{pmatrix} \cdot(\boldsymbol{k}_t, z_0, z_1) \begin{pmatrix} \boldsymbol{E}_{xy}(\boldsymbol{k}_t, z_1) \\ \eta_0 \mathbf{J} \cdot \boldsymbol{H}_{xy}(\boldsymbol{k}_t, z_1^-) \end{pmatrix} \quad (15)$$

and

$$\begin{pmatrix} \boldsymbol{F}^+(\boldsymbol{k}_t, z_{N+1}) \\ \boldsymbol{F}^-(\boldsymbol{k}_t, z_{N+1}) \end{pmatrix} = \frac{1}{2} \begin{pmatrix} \mathbf{P}_{ee} - \mathbf{W} \cdot \mathbf{P}_{me} & \mathbf{P}_{em} - \mathbf{W} \cdot \mathbf{P}_{mm} \\ \mathbf{P}_{ee} + \mathbf{W} \cdot \mathbf{P}_{me} & \mathbf{P}_{em} + \mathbf{W} \cdot \mathbf{P}_{mm} \end{pmatrix} \cdot(\boldsymbol{k}_t, z_{N+1}, z_N) \cdot \begin{pmatrix} \boldsymbol{E}_{xy}(\boldsymbol{k}_t, z_N) \\ \eta_0 \mathbf{J} \cdot \boldsymbol{H}_{xy}(\boldsymbol{k}_t, z_N^+) \end{pmatrix} \quad (16)$$

where $\mathbf{W}$ is the vacuum wave splitting operator. In these expressions the incoming transverse fields from the left and the right hand side of the slab are $\boldsymbol{F}^+(\boldsymbol{k}_t, z_0)$ and $\boldsymbol{F}^-(\boldsymbol{k}_t, z_{N+1})$, respectively. Similarly, the scattered transverse fields in the half spaces are $\boldsymbol{F}^-(\boldsymbol{k}_t, z_0)$ and $\boldsymbol{F}^+(\boldsymbol{k}_t, z_{N+1})$, respectively.

To solve the propagation problem for the entire slab, we use equations (11), (15), and (16) to express the scattered fields, $\boldsymbol{F}^-(\boldsymbol{k}_t, z_0)$ and $\boldsymbol{F}^+(\boldsymbol{k}_t, z_{N+1})$, and the doubly represented magnetic fields at the screens, $\boldsymbol{H}_{xy}(\boldsymbol{k}_t, z_n^\pm),\ n = 1, \ldots, N$, in terms of the incoming fields, $\boldsymbol{F}^+(\boldsymbol{k}_t, z_0)$ and $\boldsymbol{F}^-(\boldsymbol{k}_t, z_{N+1})$ and the electric fields at the screens, $\boldsymbol{E}_{xy}(\boldsymbol{k}_t, z_n),\ n = 1, \ldots, N$, (note that the electric field is continuous at

z_n and, therefore, it is irrelevant which side of the metallic scatterer the transverse electric field is evaluated). Finally, by equation (14), the current densities at the screens, $\boldsymbol{J}_S(\boldsymbol{k}_t, z_n),\ n = 1, \ldots, N$, can be related to the electric fields at the screens, $\boldsymbol{E}_{xy}(\boldsymbol{k}_t, z_n),\ n = 1, \ldots, N$.

To this end, we write equation (11) (for $n = 1, \ldots, N-1$) in the form[‡]

$$\begin{pmatrix} \eta_0 \mathbf{J} \cdot \boldsymbol{H}_{xy}(\boldsymbol{k}_t, z_n^+) \\ \eta_0 \mathbf{J} \cdot \boldsymbol{H}_{xy}(\boldsymbol{k}_t, z_{n+1}^-) \end{pmatrix} = \begin{pmatrix} \mathbf{P}_{mm} \cdot \mathbf{P}_{em}^{-1} & \mathbf{P}_{me} - \mathbf{P}_{mm} \cdot \mathbf{P}_{em}^{-1} \cdot \mathbf{P}_{ee} \\ \mathbf{P}_{em}^{-1} & -\mathbf{P}_{em}^{-1} \cdot \mathbf{P}_{ee} \end{pmatrix} \cdot(\boldsymbol{k}_t, z_n, z_{n+1}) \cdot \begin{pmatrix} \boldsymbol{E}_{xy}(\boldsymbol{k}_t, z_n) \\ \boldsymbol{E}_{xy}(\boldsymbol{k}_t, z_{n+1}) \end{pmatrix}$$

Hence, using equation (14),

$$\begin{aligned} \eta_0 \boldsymbol{J}_S(\boldsymbol{k}_t, z_n) \ = \ & \mathbf{A}_{nn-1}(\boldsymbol{k}_t) \cdot \boldsymbol{E}_{xy}(\boldsymbol{k}_t, z_{n-1}) \\ & + \mathbf{A}_{nn}(\boldsymbol{k}_t) \cdot \boldsymbol{E}_{xy}(\boldsymbol{k}_t, z_n) \ (n = 2, \ldots, N-1) \\ & + \mathbf{A}_{nn+1}(\boldsymbol{k}_t) \cdot \boldsymbol{E}_{xy}(\boldsymbol{k}_t, z_{n+1}) \end{aligned} \quad (17)$$

where

$$\begin{cases} \mathbf{A}_{nn-1}(\boldsymbol{k}_t) = -\mathbf{P}_{em}^{-1}(\boldsymbol{k}_t, z_{n-1}, z_n) \\ \mathbf{A}_{nn}(\boldsymbol{k}_t) = \left(\mathbf{P}_{mm} \cdot \mathbf{P}_{em}^{-1}\right)(\boldsymbol{k}_t, z_n, z_{n+1}) + \left(\mathbf{P}_{em}^{-1} \cdot \mathbf{P}_{ee}\right)(\boldsymbol{k}_t, z_{n-1}, z_n) \\ \mathbf{A}_{nn+1}(\boldsymbol{k}_t) = \left(\mathbf{P}_{me} - \mathbf{P}_{mm} \cdot \mathbf{P}_{em}^{-1} \cdot \mathbf{P}_{ee}\right)(\boldsymbol{k}_t, z_n, z_{n+1}) \end{cases} \quad (18)$$

Equation (17) is a relation between the surface current at the interior screens and the transverse electric fields at the screen and at its two neighbours. Similarly, using (14), the relations between the transverse magnetic fields the exterior screens and the transverse electric fields at the screen and its closest neighbour are found to be

$$\begin{aligned} \eta_0 \mathbf{J} \cdot \boldsymbol{H}_{xy}(\boldsymbol{k}_t, z_1^+) \ = \ & \left(\mathbf{P}_{mm} \cdot \mathbf{P}_{em}^{-1} \ \ \mathbf{P}_{me} - \mathbf{P}_{mm} \cdot \mathbf{P}_{em}^{-1} \cdot \mathbf{P}_{ee}\right)(\boldsymbol{k}_t, z_1, z_2) \\ & \cdot \begin{pmatrix} \boldsymbol{E}_{xy}(\boldsymbol{k}_t, z_1) \\ \boldsymbol{E}_{xy}(\boldsymbol{k}_t, z_2) \end{pmatrix} \end{aligned} \quad (19)$$

and

$$\begin{aligned} \eta_0 \mathbf{J} \cdot \boldsymbol{H}_{xy}(\boldsymbol{k}_t, z_N^-) \ = \ & \left(\mathbf{P}_{em}^{-1} \ \ -\mathbf{P}_{em}^{-1} \cdot \mathbf{P}_{ee}\right)(\boldsymbol{k}_t, z_{N-1}, z_N) \\ & \cdot \begin{pmatrix} \boldsymbol{E}_{xy}(\boldsymbol{k}_t, z_{N-1}) \\ \boldsymbol{E}_{xy}(\boldsymbol{k}_t, z_N) \end{pmatrix} \end{aligned} \quad (20)$$

[‡] The formula is written in an economical form, and the dependence on the parameters must be read with caution. For instance, $(\mathbf{P}_{mm} \cdot \mathbf{P}_{em}^{-1})(\boldsymbol{k}_t, z_n, z_{n+1})$ should be interpreted as $\mathbf{P}_{mm}(\boldsymbol{k}_t, z_n, z_{n+1}) \cdot \mathbf{P}_{em}^{-1}(\boldsymbol{k}_t, z_n, z_{n+1})$. This convention is used throughout this section.

On the other hand, the scattering relations (15) and (16) can be written as

$$\boldsymbol{F}^-(\boldsymbol{k}_t, z_0) = \mathbf{C}_0(\boldsymbol{k}_t) \cdot \boldsymbol{F}^+(\boldsymbol{k}_t, z_0) + \mathbf{C}_1(\boldsymbol{k}_t) \cdot \boldsymbol{E}_{xy}(\boldsymbol{k}_t, z_1) \tag{21}$$

where

$$\begin{cases} \mathbf{C}_0(\boldsymbol{k}_t) = \left((\mathbf{P}_{em} + \mathbf{W} \cdot \mathbf{P}_{mm}) \cdot (\mathbf{P}_{em} - \mathbf{W} \cdot \mathbf{P}_{mm})^{-1}\right)(\boldsymbol{k}_t, z_0, z_1) \\ \mathbf{C}_1(\boldsymbol{k}_t) = \Big(-\dfrac{1}{2}(\mathbf{P}_{em} + \mathbf{W} \cdot \mathbf{P}_{mm}) \cdot (\mathbf{P}_{em} - \mathbf{W} \cdot \mathbf{P}_{mm})^{-1} \\ \qquad \cdot (\mathbf{P}_{ee} - \mathbf{W} \cdot \mathbf{P}_{me}) + \dfrac{1}{2}(\mathbf{P}_{ee} + \mathbf{W} \cdot \mathbf{P}_{me})\Big)(\boldsymbol{k}_t, z_0, z_1) \end{cases} \tag{22}$$

This expression is a relation between the input field from the left, $\boldsymbol{F}^+(\boldsymbol{k}_t, z_0)$, and the (unknown) scattered field to the left, $\boldsymbol{F}^-(\boldsymbol{k}_t, z_0)$ which consists of both a reflected and a transmitted part, and the (unknown) electric field on the first scatterer, $\boldsymbol{E}_{xy}(\boldsymbol{k}_t, z_1)$. Similarly, at the other side of the entire slab we get

$$\boldsymbol{F}^+(\boldsymbol{k}_t, z_{N+1}) = \mathbf{D}_{N+1}(\boldsymbol{k}_t) \cdot \boldsymbol{F}^-(\boldsymbol{k}_t, z_{N+1}) + \mathbf{D}_N(\boldsymbol{k}_t) \cdot \boldsymbol{E}_{xy}(\boldsymbol{k}_t, z_N) \tag{23}$$

where

$$\begin{cases} \mathbf{D}_{N+1}(\boldsymbol{k}_t) = \left((\mathbf{P}_{em} - \mathbf{W} \cdot \mathbf{P}_{mm}) \cdot (\mathbf{P}_{em} + \mathbf{W} \cdot \mathbf{P}_{mm})^{-1}\right)(\boldsymbol{k}_t, z_{N+1}, z_N) \\ \mathbf{D}_N(\boldsymbol{k}_t) = \Big(-\dfrac{1}{2}(\mathbf{P}_{em} - \mathbf{W} \cdot \mathbf{P}_{mm}) \cdot (\mathbf{P}_{em} + \mathbf{W} \cdot \mathbf{P}_{mm})^{-1} \\ \qquad \cdot (\mathbf{P}_{ee} + \mathbf{W} \cdot \mathbf{P}_{me}) + \dfrac{1}{2}(\mathbf{P}_{ee} - \mathbf{W} \cdot \mathbf{P}_{me})\Big)(\boldsymbol{k}_t, z_{N+1}, z_N) \end{cases} \tag{24}$$

This expression is a relation between the input field from the right, $\boldsymbol{F}^-(\boldsymbol{k}_t, z_{N+1})$ and the (unknown) scattered field to the right, $\boldsymbol{F}^+(\boldsymbol{k}_t, z_{N+1})$ which consists of both a reflected and a transmitted part, and the (unknown) electric field on the last scatterer, $\boldsymbol{E}_{xy}(\boldsymbol{k}_t, z_N)$.

Moreover, from the relations (15) and (16) have the relations

$$\begin{aligned} \eta_0 \mathbf{J} \cdot \boldsymbol{H}_{xy}(\boldsymbol{k}_t, z_1^-) &= 2(\mathbf{P}_{em} - \mathbf{W} \cdot \mathbf{P}_{mm})^{-1}(\boldsymbol{k}_t, z_0, z_1) \cdot \boldsymbol{F}^+(\boldsymbol{k}_t, z_0) \\ &- \Big((\mathbf{P}_{em} - \mathbf{W} \cdot \mathbf{P}_{mm})^{-1} \cdot (\mathbf{P}_{ee} - \mathbf{W} \cdot \mathbf{P}_{me})\Big)(\boldsymbol{k}_t, z_0, z_1) \cdot \boldsymbol{E}_{xy}(\boldsymbol{k}_t, z_1) \end{aligned} \tag{25}$$

and

$$\begin{aligned} \eta_0 \mathbf{J} \cdot \boldsymbol{H}_{xy}(\boldsymbol{k}_t, z_N^+) &= 2(\mathbf{P}_{em} + \mathbf{W} \cdot \mathbf{P}_{mm})^{-1}(\boldsymbol{k}_t, z_{N+1}, z_N) \cdot \boldsymbol{F}^-(\boldsymbol{k}_t, z_{N+1}) \\ &- \Big((\mathbf{P}_{em} - \mathbf{W} \cdot \mathbf{P}_{mm})^{-1} \cdot (\mathbf{P}_{ee} + \mathbf{W} \cdot \mathbf{P}_{me})\Big)(\boldsymbol{k}_t, z_{N+1}, z_N) \cdot \boldsymbol{E}_{xy}(\boldsymbol{k}_t, z_N) \end{aligned} \tag{26}$$

at the exterior screens.

To proceed, we divide the analysis in two separate paths, depending on whether there are one screen ($N = 1$) or whether there are several ($N > 1$). These cases are different due to the fact that in the first case the screen has the two half spaces next to the screen. In the second case there is always a screen as a neighbour.

5.1. Special Case — Several Screens ($N > 1$)

The goal of this section is to find the expression that relates the surface currents on the screens, $\boldsymbol{J}_S(\boldsymbol{k}_t, z_n)$, to the electric field on the screens, $\boldsymbol{E}_{xy}(\boldsymbol{k}_t, z_n)$, and to the excitations of the entire slab, $\boldsymbol{F}^+(\boldsymbol{k}_t, z_0)$ and $\boldsymbol{F}^-(\boldsymbol{k}_t, z_{N+1})$.

We express the surface current at the first screen by a combination of the equations (19) and (25). The result is

$$\begin{aligned}\eta_0 \boldsymbol{J}_S(\boldsymbol{k}_t, z_1) \;=\; & \mathbf{A}_{11}(\boldsymbol{k}_t) \cdot \boldsymbol{E}_{xy}(\boldsymbol{k}_t, z_1) + \mathbf{A}_{12}(\boldsymbol{k}_t) \cdot \boldsymbol{E}_{xy}(\boldsymbol{k}_t, z_2) \\ & + \mathbf{A}_{10}(\boldsymbol{k}_t) \cdot \boldsymbol{F}^+(\boldsymbol{k}_t, z_0) \end{aligned} \tag{27}$$

where

$$\begin{cases} \mathbf{A}_{11}(\boldsymbol{k}_t) = (\boldsymbol{P}_{mm} \cdot \boldsymbol{P}_{em}^{-1})(\boldsymbol{k}_t, z_1, z_2) \\ \qquad\qquad + \left((\mathbf{P}_{em} - \mathbf{W} \cdot \mathbf{P}_{mm})^{-1} \cdot (\mathbf{P}_{ee} - \mathbf{W} \cdot \mathbf{P}_{me})\right)(\boldsymbol{k}_t, z_0, z_1) \\ \mathbf{A}_{12}(\boldsymbol{k}_t) = (\boldsymbol{P}_{me} - \mathbf{P}_{mm} \cdot \boldsymbol{P}_{em}^{-1} \cdot \mathbf{P}_{ee})(\boldsymbol{k}_t, z_1, z_2) \\ \mathbf{A}_{10}(\boldsymbol{k}_t) = -2(\mathbf{P}_{em} - \mathbf{W} \cdot \mathbf{P}_{mm})^{-1}(\boldsymbol{k}_t, z_0, z_1) \end{cases}$$

By combining equations (20) and (26) we get the surface current at the last screen

$$\begin{aligned}\eta_0 \boldsymbol{J}_S(\boldsymbol{k}_t, z_N) = & \mathbf{A}_{NN-1}(\boldsymbol{k}_t) \cdot \boldsymbol{E}_{xy}(\boldsymbol{k}_t, z_{N-1}) + \mathbf{A}_{NN}(\boldsymbol{k}_t) \cdot \boldsymbol{E}_{xy}(\boldsymbol{k}_t, z_N) \\ & + \mathbf{A}_{NN+1}(\boldsymbol{k}_t) \cdot \boldsymbol{F}^-(\boldsymbol{k}_t, z_{N+1}) \end{aligned} \tag{28}$$

where

$$\begin{cases} \mathbf{A}_{NN-1}(\boldsymbol{k}_t) = -\mathbf{P}_{em}^{-1}(\boldsymbol{k}_t, z_{N-1}, z_N) \\ \mathbf{A}_{NN}(\boldsymbol{k}_t) = (\mathbf{P}_{me}^{-1} \cdot \mathbf{P}_{ee})(\boldsymbol{k}_t, z_{N-1}, z_N) \\ \qquad\qquad - ((\mathbf{P}_{em} + \mathbf{W} \cdot \mathbf{P}_{mm})^{-1} \cdot (\mathbf{P}_{ee} + \mathbf{W} \cdot \mathbf{P}_{me}))(\boldsymbol{k}_t, z_{N+1}, z_N) \\ \mathbf{A}_{NN+1}(\boldsymbol{k}_t) = 2(\mathbf{P}_{em} + \mathbf{W} \cdot \mathbf{P}_{mm})^{-1}(\boldsymbol{k}_t, z_{N+1}, z_N) \end{cases}$$

Equations (17), (27), and (28) constitutes a set of equations that can be combined into a single expression ($n = 1, \ldots, N$)

$$\eta_0 \boldsymbol{J}_S(\boldsymbol{k}_t, z_n) = \sum_{m=1}^{N} \mathbf{A}_{nm}(\boldsymbol{k}_t) \cdot \boldsymbol{E}_{xy}(\boldsymbol{k}_t, z_m)$$

$$+\delta_{n1}\mathbf{A}_{10}(\boldsymbol{k}_t)\cdot\boldsymbol{F}^{+}(\boldsymbol{k}_t,z_0)+\delta_{nN}\mathbf{A}_{NN+1}(\boldsymbol{k}_t)\cdot\boldsymbol{F}^{-}(\boldsymbol{k}_t,z_{N+1}) \tag{29}$$

which is the starting point for the Galerkin procedure. Note that the sum in the expression above only has at most three terms, since all matrices $\boldsymbol{A}_{nm}$ vanish if $m \neq n,\ n \pm 1$. The equation (29) can be written in compact form by composing the square $(2N \times 2N)$ matrix of band block type

$$\mathbf{A}(\boldsymbol{k}t) = (\mathbf{A}_{nm}(\boldsymbol{k}_t))$$

from the square (2×2) matrices $\boldsymbol{A}_{nm}(\boldsymbol{k}_t),\ m,n = 1,\ldots,N$, *i.e.*,

$$\mathbf{A} = \begin{pmatrix} \mathbf{A}_{11} & \mathbf{A}_{12} & \mathbf{0} & \cdots & \cdots & \cdots \\ \mathbf{A}_{21} & \mathbf{A}_{22} & \mathbf{A}_{23} & \mathbf{0} & \cdots & \cdots \\ \mathbf{0} & \mathbf{A}_{32} & \mathbf{A}_{33} & \mathbf{A}_{34} & \mathbf{0} & \cdots \\ \vdots & \vdots & \vdots & \ddots & \vdots & \vdots \\ \cdots & \cdots & \mathbf{0} & \mathbf{A}_{N-1N-2} & \mathbf{A}_{N-1N-1} & \mathbf{A}_{N-1N} \\ \cdots & \cdots & \cdots & \mathbf{0} & \mathbf{A}_{NN-1} & \mathbf{A}_{NN} \end{pmatrix}$$

The simple block band characteristics of the matrix $\boldsymbol{A}(\boldsymbol{k}_t)$ have several advantages that is used below. Moreover, by introducing the inverse $\mathbf{B} = \mathbf{A}^{-1}$ of $\mathbf{A}$, which is not of band block type, and decomposing this matrix as

$$\mathbf{B}(\boldsymbol{k}_t) = (\mathbf{B}_{nm}(\boldsymbol{k}_t))$$

where the dimension of the block matrices $\mathbf{B}_{nm}(\boldsymbol{k}_t),\ m,n = 1,\ldots,N$, is 2×2, equation (29) can be inverted and the transverse electric field $\boldsymbol{E}_{xy}(\boldsymbol{k}_t, z_n)$ can be found in terms of the surface currents $\boldsymbol{J}_S(\boldsymbol{k}_t, z_m)$:

$$\begin{aligned}\boldsymbol{E}_{xy}(\boldsymbol{k}_t,z_n) = &\sum_{m=1}^{N}\mathbf{B}_{nm}(\boldsymbol{k}_t)\cdot\eta_0\boldsymbol{J}_S(\boldsymbol{k}_t,z_m) \\ &-\mathbf{B}_{n0}(\boldsymbol{k}_t)\cdot\boldsymbol{F}^{+}(\boldsymbol{k}_t,z_0)-\mathbf{B}_{nN+1}(\boldsymbol{k}_t)\cdot\boldsymbol{F}^{-}(\boldsymbol{k}_t,z_{N+1})\end{aligned} \tag{30}$$

where $\mathbf{B}_{n0}(\boldsymbol{k}_t) = \mathbf{B}_{n1}(\boldsymbol{k}_t)\cdot\mathbf{A}_{10}(\boldsymbol{k}_t)$ and $\mathbf{B}_{nN+1}(\boldsymbol{k}_t) = \mathbf{B}_{nN}(\boldsymbol{k}_t)\cdot\mathbf{A}_{NN+1}(\boldsymbol{k}_t)$.

Equations (29) and (30) constitute the final set of equations for the case of several screen. The first equation, (29), is the most suitable for the analysis of the aperture case, while the second one, (30), is more adapted to the the patch case. These observations are exploited further below.

5.2. Special Case — One Screen ($N = 1$)

The case of one screen is special in that the screen has a half space on each side of it. There are, therefore, no interior screens, and we need to consider this case separately. Again, the goal of this section is to find the expression that relates the surface current on the screen, $\boldsymbol{J}_S(\boldsymbol{k}_t, z_1)$, to the electric field on the screen, $\boldsymbol{E}_{xy}(\boldsymbol{k}_t, z_1)$, and to the excitations of the entire slab, $\boldsymbol{F}^+(\boldsymbol{k}_t, z_2)$ and $\boldsymbol{F}^-(\boldsymbol{k}_t, z_2)$.

We let $N = 1$ and combine (25) and (26) to get

$$\begin{aligned}\eta_0 \boldsymbol{J}_S(\boldsymbol{k}_t, z_1) \;=\; & \mathbf{A}_{11}(\boldsymbol{k}_t) \cdot \boldsymbol{E}_{xy}(\boldsymbol{k}_t, z_1) + \mathbf{A}_{10}(\boldsymbol{k}_t) \cdot \boldsymbol{F}^+(\boldsymbol{k}_t, z_0) \\ & + \mathbf{A}_{12}(\boldsymbol{k}_t) \cdot \boldsymbol{F}^-(\boldsymbol{k}_t, z_2)\end{aligned} \tag{31}$$

where

$$\left\{\begin{array}{l} \mathbf{A}_{11}(\boldsymbol{k}_t) = -\left((\boldsymbol{P}_{em} + \mathbf{W} \cdot \boldsymbol{P}_{mm})^{-1} \cdot (\mathbf{P}_{ee} + \mathbf{W} \cdot \mathbf{P}_{me})\right)(\boldsymbol{k}_t, z_2, z_1) \\ \qquad\qquad + \left((\mathbf{P}_{em} - \mathbf{W} \cdot \mathbf{P}_{mm})^{-1} \cdot (\mathbf{P}_{ee} - \mathbf{W} \cdot \mathbf{P}_{me})\right)(\boldsymbol{k}_t, z_0, z_1) \\ \mathbf{A}_{12}(\boldsymbol{k}_t) = 2(\boldsymbol{P}_{em} + \mathbf{W} \cdot \mathbf{P}_{mm})^{-1}(\boldsymbol{k}_t, z_2, z_1) \\ \mathbf{A}_{10}(\boldsymbol{k}_t) = -2(\mathbf{P}_{em} - \mathbf{W} \cdot \mathbf{P}_{mm})^{-1}(\boldsymbol{k}_t, z_0, z_1) \end{array}\right. \tag{32}$$

Equation (31) is a special case of (29) for one screen. It is, however, not possible to obtain this case from the general case.

The relation (31) can be inverted and the transverse electric field $\boldsymbol{E}_{xy}(\boldsymbol{k}_t, z_1)$ can be found in terms of the surface currents $\boldsymbol{J}_S(\boldsymbol{k}_t, z_1)$. The result is

$$\begin{aligned}\boldsymbol{E}_{xy}(\boldsymbol{k}_t, z_1) \;=\; & \mathbf{B}_{11}(\boldsymbol{k}_t) \cdot \eta_0 \boldsymbol{J}_S(\boldsymbol{k}_t, z_1) - \mathbf{B}_{10}(\boldsymbol{k}_t) \cdot \boldsymbol{F}^+(\boldsymbol{k}_t, z_0) \\ & - \mathbf{B}_{12}(\boldsymbol{k}_t) \cdot \boldsymbol{F}^-(\boldsymbol{k}_t, z_2)\end{aligned} \tag{33}$$

where

$$\left\{\begin{array}{l} \mathbf{B}_{11}(\boldsymbol{k}_t) = \mathbf{A}_{11}(\boldsymbol{k}_t)^{-1} \\ \mathbf{B}_{10}(\boldsymbol{k}_t) = \mathbf{B}_{11}(\boldsymbol{k}_t) \cdot \mathbf{A}_{10}(\boldsymbol{k}_t) \\ \mathbf{B}_{12}(\boldsymbol{k}_t) = \mathbf{B}_{11}(\boldsymbol{k}_t) \cdot \mathbf{A}_{12}(\boldsymbol{k}_t) \end{array}\right.$$

Equation (33) is a special case of (30) for the one screen case.

5.2.1. Connection to Reflection Dyadics Representation

The conventional way of solving scattering problems in planar geometries is by introducing the appropriate reflection and transmission dyadics of the slabs — see the references cited in the introduction. As already should be obvious from above, this approach is not used in this paper. However, the reflection and the transmission dyadics can

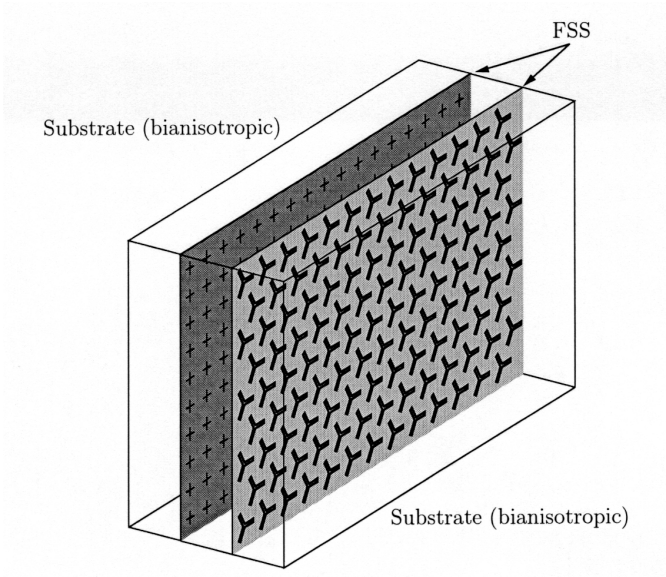

Figure 2. The geometry of a slab with two patch FSS supported by arbitrary, general slabs.

be identified from our approach for the one screen case. We like to stress that there are no advantages obtained in the numerical solution of the problem by such an identification, but there could be some pedagogical advantages in showing the connections to the more standard procedure. This identification parallels the connection in transmission line theory between the voltage-current or transmission (ABCD) matrix formulation and the scattering matrix formulation [3, 14]. The technical details in this identifications are omitted here, and we refer the reader to Ref. [10] for the details.

6. THE PERIODIC CASE — FSS

In the previous section, we analysed the case of a finite number of patches or apertures of arbitrary shape on each screen. We now let the number of patches or apertures on each screen be infinite, and, moreover, they are arranged in a periodic pattern on each screen. This situation comprises the important application of frequency selective surfaces or structures (FSS) [13].

To this end, we assume that all the patches or apertures on scatterer S_n are periodically distributed over the plane $z = z_n$ for

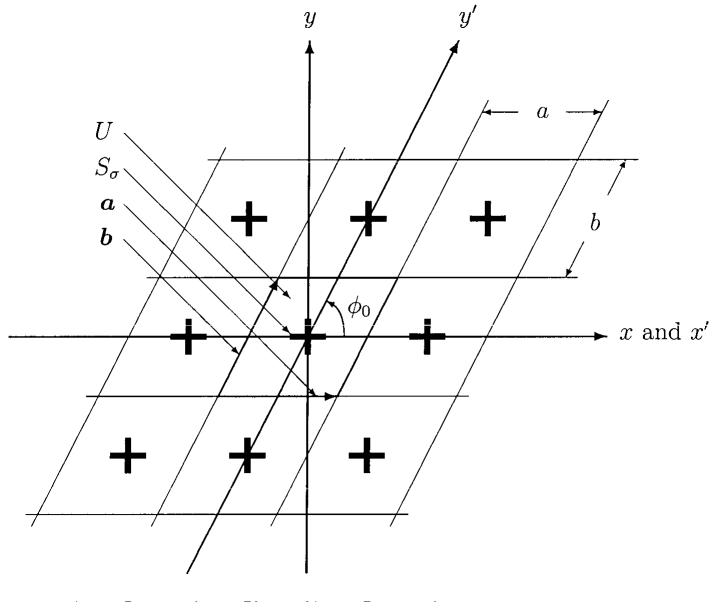

Figure 3. The unit cell U (patch case) generated by $\boldsymbol{a}$ and $\boldsymbol{b}$ with lengths $a = |\boldsymbol{a}|$ and $b = |\boldsymbol{b}|$.

$n = 1, 2, \ldots, N$, see also Figure 2. The periodicity is assumed to be the same or commensurate on all screens. Consequently, a unit cell relevant for all the screens can by defined by two linearly independent, lateral vectors, say a $\boldsymbol{a} \in \mathbb{R}^2$ and $\boldsymbol{b} \in \mathbb{R}^2$ with lengths $a = |\boldsymbol{a}|$ and $b = |\boldsymbol{b}|$, respectively, see Figure 3. The periodic pattern can be obliquely oriented and ϕ_0 denotes the (smallest) angle between the axes of periodicity defined by $\cos\phi_0 = \boldsymbol{a} \cdot \boldsymbol{b}/(ab)$. We denote the unit cell by U, its area $A_U = |\boldsymbol{a} \times \boldsymbol{b}| = ab \sin\phi_0$, and the metallic parts in the unit cell by S_σ.

In the previous sections, the excitation was arbitrary and there could be sources on both sides of the slab, *i.e.*, in the regions $z < z_0$ and $z > z_{N+1}$ We now assume the incident wave to be a plane wave only from the left, *i.e.*, $\boldsymbol{F}^-(\boldsymbol{k}_t, z_{N+1}) = \boldsymbol{0}$. Explicitly, we have

$$\boldsymbol{E}^i(\boldsymbol{r}) = \boldsymbol{E}^i_0 e^{i\boldsymbol{k}^i \cdot \boldsymbol{r}}$$

where $\boldsymbol{k}^i = k_0 \hat{\boldsymbol{k}}^i$ is the constant real wave vector of the incident wave, and $\boldsymbol{E}^i_0$ is a constant complex vector, such that $\boldsymbol{E}^i_0 \cdot \boldsymbol{k}^i = 0$. The Fourier transform of the lateral part of this field evaluated at $z =$ constant is

$$\boldsymbol{F}^+(\boldsymbol{k}_t, z_0) e^{ik^i_z(z-z_0)} = \boldsymbol{E}^i_{xy}(\boldsymbol{k}_t, z) = 4\pi^2 \boldsymbol{E}^i_{0xy} e^{ik^i_z z} \delta^2(\boldsymbol{k}_t - \boldsymbol{k}^i_t) \qquad (34)$$

where the wave vector has been decomposed in lateral and longitudinal parts as $\boldsymbol{k}^i = \boldsymbol{k}_t^i + \hat{\boldsymbol{z}} k_z^i$, *i.e.*, $k_z^i = \boldsymbol{k}^i \cdot \hat{\boldsymbol{z}}$ and $\boldsymbol{k}_t^i = \mathbf{I}_2 \cdot \boldsymbol{k}^i$. The components of $\boldsymbol{k}^i$ in the x- and y-directions are denoted by k_x^i and k_y^i, respectively, *i.e.*, $\boldsymbol{k}_t^i = \hat{\boldsymbol{x}} k_x^i + \hat{\boldsymbol{y}} k_y^i$, and the spherical angles of $\boldsymbol{k}^i$ are denoted θ (polar angle) and ϕ (azimuth angle), *i.e.*, $\boldsymbol{k}^i = k_0(\hat{\boldsymbol{x}} \sin\theta\cos\phi + \hat{\boldsymbol{y}} \sin\theta\sin\phi + \hat{\boldsymbol{z}}\cos\theta)$.

To apply the results from the previous sections we need to find the relations between the Fourier transformed quantities used above and the Fourier coefficient of the pertinent periodic quantities that are appropriate in this section. To this end, Floquet's theorem [6] is applied. Consequently, the electric and magnetic fields and the current densities can be expanded in infinite exponential series with (lateral) wave numbers, which for the special geometry in Figure 3, where $\boldsymbol{a} = \hat{\boldsymbol{x}} a$ and $\boldsymbol{b} = \hat{\boldsymbol{x}} b\cos\phi_0 + \hat{\boldsymbol{y}} b \sin\phi_0$ are ($\mathbb{Z}$ denotes the set of integers)

$$\boldsymbol{k}_{mn} = \hat{\boldsymbol{x}}\left(\frac{2\pi m}{a} + k_x^i\right) + \hat{\boldsymbol{y}}\left(\frac{2\pi n}{b\sin\phi_0} - \frac{2\pi m}{a}\cot\phi_0 + k_y^i\right), \ m,n \in \mathbb{Z} \tag{35}$$

Notice that $\boldsymbol{k}_{00} = \boldsymbol{k}_t^i$.

Applying Floquet's theorem [6] to the induced surface current densities at the screens, $\boldsymbol{J}_S(\boldsymbol{\rho}, z_j) = \mathbf{J} \cdot (\boldsymbol{H}(\boldsymbol{\rho}, z_j^+) - \boldsymbol{H}(\boldsymbol{\rho}, z_j^-))$, which in non-zero on the metallic parts, S_σ, and zero elsewhere on the plane $z = z_j$, gives

$$\boldsymbol{J}_S(\boldsymbol{\rho}, z_j) = \frac{1}{A_U} \sum_{m,n=-\infty}^{\infty} \boldsymbol{J}_S|_U(\boldsymbol{k}_{mn}, z_j) e^{i\boldsymbol{k}_{mn}\cdot\boldsymbol{\rho}}, \ j = 1,2,\ldots,N, \ \boldsymbol{\rho} \in \mathbb{R}^2$$

where the lateral wave numbers $\boldsymbol{k}_{mn}$ are given by equation (35), and the coefficient $\boldsymbol{J}_S|_U(\boldsymbol{k}_{mn}, z_j)$ is the lateral Fourier transform of $\boldsymbol{J}_S(\boldsymbol{\rho}, z_j)$ restricted to the unit cell U and evaluated at $\boldsymbol{k}_{mn}$, *i.e.*,

$$\boldsymbol{J}_S|_U(\boldsymbol{k}_{mn}, z_j) = \iint_U \boldsymbol{J}_S(\boldsymbol{\rho}, z_j) e^{-i\boldsymbol{k}_{mn}\cdot\boldsymbol{\rho}} dxdy, \quad j = 1,2,\ldots,N$$

Notice that this quantity is identical to the Fourier coefficient of the periodic function $\boldsymbol{J}_S(\boldsymbol{\rho}, z_j) e^{-i\boldsymbol{k}_t^i\cdot\boldsymbol{\rho}}$. The symbol $|_U$ is used here and below to emphasise that the quantity is a lateral Fourier transform of an aperiodic quantity with support in the unit cell U and to distinguish between $\boldsymbol{J}_S(\boldsymbol{k}_t, z_j)$ and $\boldsymbol{J}_S|_U(\boldsymbol{k}_{mn}, z_j)$. Consequently, the connection between the lateral Fourier transforms of the surface current densities,

$\boldsymbol{J}_S(\boldsymbol{k}_t, z_j)$, and its restriction to the unit cell, $\boldsymbol{J}_S|_U(\boldsymbol{k}_{mn}, z_j)$, is, cf. (2)

$$\boldsymbol{J}_S(\boldsymbol{k}_t, z_j) = \frac{4\pi^2}{A_U} \sum_{m,n=-\infty}^{\infty} \boldsymbol{J}_S|_U(\boldsymbol{k}_{mn}, z_j)\delta^2(\boldsymbol{k}_t - \boldsymbol{k}_{mn}), \quad j = 1, 2, \ldots, N \tag{36}$$

This connection can now be used in the results in the previous sections.

Similarly, applying Floquet's theorem to the lateral electric fields at the screens, $\boldsymbol{E}_{xy}(\boldsymbol{\rho}, z_j)$, yields

$$\boldsymbol{E}_{xy}(\boldsymbol{\rho}, z_j) = \frac{1}{A_U} \sum_{m,n=-\infty}^{\infty} \boldsymbol{E}_{xy}|_U(\boldsymbol{k}_{mn}, z_j)e^{i\boldsymbol{k}_{mn}\cdot\boldsymbol{\rho}}, \quad j = 1, 2, \ldots, N$$

and

$$\boldsymbol{E}_{xy}(\boldsymbol{k}_t, z_j) = \frac{4\pi^2}{A_U} \sum_{m,n=-\infty}^{\infty} \boldsymbol{E}_{xy}|_U(\boldsymbol{k}_{mn}, z_j)\delta^2(\boldsymbol{k}_t - \boldsymbol{k}_{mn}),\ j = 1, 2, \ldots, N \tag{37}$$

Finally, since $\boldsymbol{k}_t^i = \boldsymbol{k}_{00}$, the excitation from the left (34) can be written as

$$\boldsymbol{F}^+(\boldsymbol{k}_t, z_0) = 4\pi^2 \boldsymbol{F}^+(\boldsymbol{k}_{00}, z_0)\delta^2(\boldsymbol{k}_t - \boldsymbol{k}_{00}) \tag{38}$$

where $\boldsymbol{F}^+(\boldsymbol{k}_{00}, z_0) = \boldsymbol{E}_{0xy}^i e^{ik_z^i z_0}$.

In this section, we analyse only the patch case in some detail. The corresponding analysis of the aperture case is found in *e.g.*, [10]. Substituting equations (36), (37), and (38) into the relation (30) between the electric fields, the surface current densities, and the excitation from the left gives

$$\begin{aligned}\boldsymbol{E}_{xy}|_U(\boldsymbol{k}_{mn}, z_j) = &\sum_{k=1}^{N} \mathbf{B}_{jk}(\boldsymbol{k}_{mn}) \cdot \eta_0 \boldsymbol{J}_S|_U(\boldsymbol{k}_{mn}, z_k) \\ &- A_U \mathbf{B}_{j0}(\boldsymbol{k}_{00}) \cdot \boldsymbol{F}^+(\boldsymbol{k}_{00}, z_0)\delta_{m0}\delta_{n0},\ j = 1, 2, \ldots, N\end{aligned} \tag{39}$$

where the **B**-matrices were defined in Section 5. This equation holds when $N > 1$. When $N = 1$, plugging into (33) gives an identical result

$$\begin{aligned}\boldsymbol{E}_{xy}|_U(\boldsymbol{k}_{mn}, z_1) \ = \ &\mathbf{B}_{11}(\boldsymbol{k}_{mn}) \cdot \eta_0 \boldsymbol{J}_S|_U(\boldsymbol{k}_{mn}, z_1) \\ &- A_U \mathbf{B}_{10}(\boldsymbol{k}_{00}) \cdot \boldsymbol{F}^+(\boldsymbol{k}_{00}, z_0)\delta_{m0}\delta_{n0}\end{aligned}$$

The current density $\boldsymbol{J}_S(\boldsymbol{\rho}, z_j)$ can be expanded with arbitrary precision in a pertinent complete set of entire domain or local basis functions

$\boldsymbol{j}_p(\boldsymbol{\rho}, z_j)$ (supported on the patches), *i.e.*,

$$\boldsymbol{J}_S(\boldsymbol{\rho}, z_j) = \sum_{p\in\chi} C_p^j \boldsymbol{j}_p(\boldsymbol{\rho}, z_j), \quad j = 1, 2, \ldots, N;\ \boldsymbol{\rho} \in U$$

where χ is a (countable) set of indices and the scalars C_p^j are the unknown expansion coefficients. It suffices to define the basis functions $\boldsymbol{j}_p(\boldsymbol{\rho}, z_j)$ in the unit cell U. The lateral Fourier transform of this expansion is

$$\boldsymbol{J}_S|_U(\boldsymbol{k}_{mn}, z_j) = \sum_{p\in\chi} C_p^j \boldsymbol{j}_p(\boldsymbol{k}_{mn}, z_j), \quad j = 1, 2, \ldots, N$$

where

$$\boldsymbol{j}_p(\boldsymbol{k}_{mn}, z_j) = \iint\limits_U \boldsymbol{j}_p(\boldsymbol{\rho}, z_j) e^{i\boldsymbol{k}_{mn}\cdot\boldsymbol{\rho}} dxdy, \quad j = 1, 2, \ldots, N;\ p \in \chi$$

We assume that an appropriate set of weight functions $\boldsymbol{w}_p(\boldsymbol{\rho}, z_j)$ (supported on the patches) has been defined. In the Galerkin's method the functions $\boldsymbol{j}_p(\boldsymbol{\rho}, z_j)$ are used. The lateral Fourier transform of the weight functions $\boldsymbol{w}_p(\boldsymbol{\rho}, z_j)$ is defined as

$$\boldsymbol{w}_p(\boldsymbol{k}_{mn}, z_j) = \iint\limits_U \boldsymbol{w}_p(\boldsymbol{\rho}, z_j) e^{-i\boldsymbol{k}_{mn}\cdot\boldsymbol{\rho}} dxdy, \quad j = 1, 2, \ldots, N$$

The starting point in the Galerkin's method is the identity

$$\iint\limits_U \boldsymbol{w}_p(\boldsymbol{\rho}, z_j)^* \cdot \boldsymbol{E}_{xy}(\boldsymbol{\rho}, z_j) dxdy = 0, \quad j = 1, 2, \ldots, N;\ p \in \chi$$

and modifying the Parseval theorem for Fourier series to Floquet expansions gives

$$\sum_{m,n=-\infty}^{\infty} \boldsymbol{w}_p(\boldsymbol{k}_{mn}, z_j)^* \cdot \boldsymbol{E}_{xy}|_U(\boldsymbol{k}_{mn}, z_j) = 0,\ j = 1, 2, \ldots, N;\ p \in \chi$$

in which equation (39) can be substituted and a system of equations for the unknown C_p^j is obtained. Specifically,

$$\begin{aligned} &\sum_{m,n=-\infty}^{\infty} \boldsymbol{w}_p(\boldsymbol{k}_{mn}, z_j)^* \cdot \sum_{k=1}^{N} \mathbf{B}_{jk}(\boldsymbol{k}_{mn}) \cdot \eta_0 \sum_{q\in\chi} C_q^k \boldsymbol{j}_q(\boldsymbol{k}_{mn}, z_k) \\ &= A_U \boldsymbol{w}_p(\boldsymbol{k}_{00}, z_j)^* \cdot \mathbf{B}_{j0}(\boldsymbol{k}_{00}) \cdot \boldsymbol{F}^+(\boldsymbol{k}_{00}, z_0),\ j = 1, 2, \ldots, N;\ p \in \chi \end{aligned}$$

If χ is an infinite set of indices, the above equation is an infinite system of linear equations for the unknown current coefficients C_q^k From the solution of the Galerkin method presented in this section the reflected and the transmitted fields are easily computed. The details in these computations are found in Ref. [10].

7. NUMERICAL EXAMPLES

In this section, we illustrate the algorithms presented above. The code is verified by comparisons with the Periodic Method of Moment program (PMM) [13] and with scattering matrix formulation [4, 5, 16].

In Figure 4, we depict the reflection and transmission coefficients for a skewed array of dipoles. This geometry is not intended to be useful in applications, but it is used to verify the implementation of the

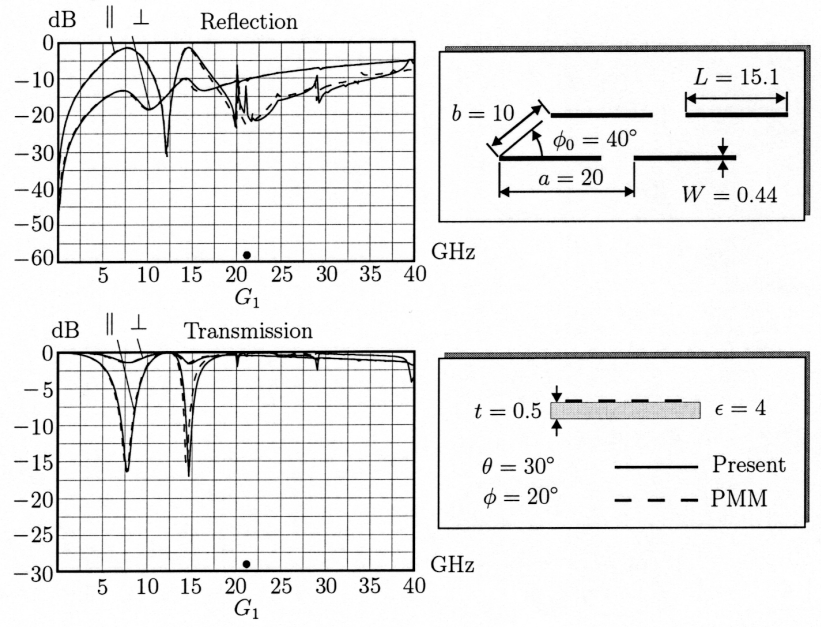

Figure 4. The reflection and transmission coefficients for a skewed array of dipoles. The onset of the grating lobes is at 21.3 GHz. The dashed curves are computed by the Periodic Method of Moment program (PMM) with 3 piecewise sinusoidal modes taken into account. The solid curves are computed by the present method using 3 basis functions, namely 2 even (cosine) and 1 odd (sine) dipole basis function. Moreover, $(2 \times 5 + 1)^2$ Floquet modes are included.

present method. The results are compared with the Periodic Method of Moment program (PMM) [13]. The agreement is excellent.

In Figure 5, the reflection coefficient for a gangbuster FSS type 3 [8] is shown. For parallel polarization, the electric field is parallel to the linear dipoles. Thus, for parallel polarization, the elements will resonate when the length of the dipole arms is about $\lambda/2$, where λ is the wavelength in the substrate. However, for orthogonal polarization, the electric field is orthogonal to the dipole arms, which means that the reflected field is scattered from the substrate alone. The first resonance of the substrate occurs when the thickness of the substrate is $\lambda_0/(2\sqrt{\epsilon - \sin^2\theta})$, where λ_0 is the wavelength in vacuum. For the data in Figure 5, this resonance occurs at approximately 6.1 GHz. In the figure, the present method is compared to the scattering matrix method

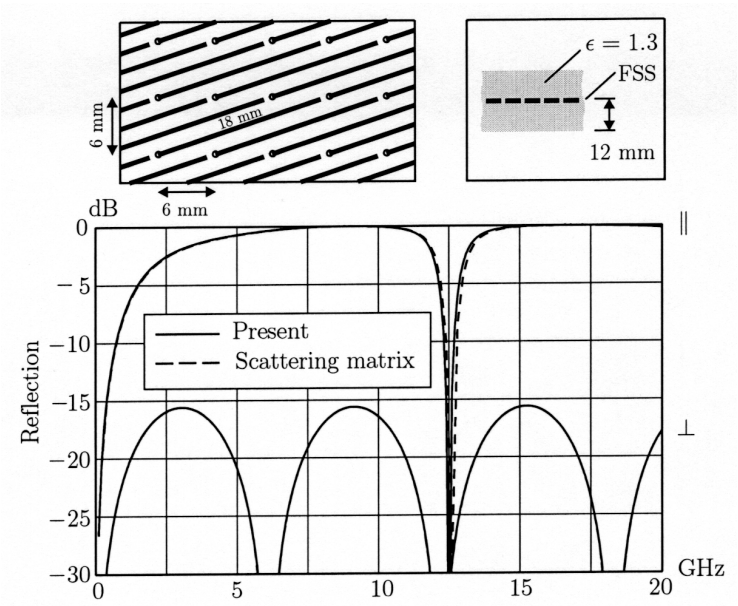

Figure 5. The reflection coefficient for a gangbuster FSS type 3 [8]. The length of the dipole arms is 18 mm, while the width is 0.5 mm. The plane of incidence is parallel to the dipoles (*i.e.*, $\phi = 18.4°$), and the angle of incidence is $\theta = 30°$. The solid curve is computed with the present method using 3 basis functions and $(2\times5+1)^2$ Floquet modes. The dashed curve is computed by the scattering matrix approach [4, 5, 16] using scattering matrices of the size $2(2\times N+1)^2\times 2(2\times N+1)^2$, with $N = 4$, *i.e.*, interaction modes up to order $N = 4$ are included.

[4, 5, 16]. Both methods agree very well. However, the computation times differ substantially. A rough estimate of the difference in evaluation time between the computations shown in Figure 5 is that the present method is more than 200 times faster than the traditional scattering matrix method. More numerical experiments have to be made in order to see whether this reduction of computation time is true in general.

8. CONCLUSIONS

A new powerful method to compute the scattering properties in planar geometries with planar metal inclusions has been presented in this paper. The method employs the propagator technique [15], which is thoroughly discussed. The main advantage with this method is that all effects of the complex interaction between the metal inclusions and the materials are included in the formulation. This type of geometry can also be analysed with other methods, *e.g.*, the Green's function method [9], but the present method is superior in its systematic structure. As a consequence, there is no need to identify the numerous reflection and transmission dyadics of the individual bianisotropic slabs that support the metal inclusions and, moreover, no cascade procedure is needed.

Several extensions of the method presented in this paper are possible. The Green's dyadic for a geometry depicted in Figure 1 is straightforward to compute and these results are reported elsewhere. Other boundary condition, such as the perfectly conducting ground plane is treated in [11]. The propagators are also an excellent instrument for the analysis of possible surface waves in the slab. This analysis is postponed to a separate paper, see also [11].

ACKNOWLEDGMENT

The work reported in this paper is supported by grants from the Swedish Defence Materiel Administration (FMV) and by the Swedish Foundation for Strategic Research (SSF), which are gratefully acknowledged.

REFERENCES

1. Bjorken, J. D. and S. D. Drell, *Relativistic Quantum Mechanics*, McGraw-Hill, New York, 1964.
2. Chew, W. C., *Waves and Fields in Inhomogeneous Media,* IEEE Press, Piscataway, NJ, 1995.

3. Collin, R. E., *Foundations for Microwave Engineering*, second edition, McGraw-Hill, New York, 1992.
4. Cwik, T. A. and R. Mittra, "The cascade connection of planar periodic surfaces and lossy dielectric layers to form an arbitrary periodic screen," *IEEE Trans. Antennas Propagat.*, Vol. 35, No. 12, 1397–1405, December 1987.
5. Cwik, T. A. and R. Mittra, "Correction to 'The cascade connection of planar periodic surfaces and lossy dielectric layers to form an arbitrary periodic screen'," *IEEE Trans. Antennas Propagat.*, Vol. 36, No. 9, 1335, September 1988.
6. Ishimaru, A., *Electromagnetic Wave Propagation, Radiation, and Scattering*, Prentice-Hall, Inc., Englewood Cliffs, New Jersey, 1991.
7. Kong, J. A., *Electromagnetic Wave Theory*, John Wiley & Sons, New York, 1986.
8. Kornbau, T. W., "Analysis of periodic arrays of rotated linear dipoles, rotated crossed dipoles, and of biplanar dipole arrays in dielectric," Ph.D. thesis, The ElectroScience Laboratory, The Ohio State University, Department of Electrical Engineering, Columbus, Ohio 43212, USA, 1984.
9. Kristensson, G., M. Åkerberg, and S. Poulsen, "Scattering from a frequency selective surface supported by a bianisotropic substrate," *Progress In Electromagnetics Research*, PIER 35, 83–114, 2001.
10. Kristensson, G., S. Poulsen, and S. Rikte, "Propagators and scattering of electromagnetic waves in planar bianisotropic slabsan application to frequency selective structures," *IEE Proc. — Microwaves, Antennas and Propagation*, Vol. 150, No. 6, 477–483, 2003.
11. Kristensson, G., P. Waller, and A. Derneryd, "Radiation efficiency and surface waves for patch antennas on inhomogeneous substrates," Technical Report LUTEDX/(TEAT-7100)/1-48/(2001), Lund Institute of Technology, Department of Electroscience, P.O. Box 118, S-221 00 Lund, Sweden, 2001. `http://www.es.1th.se`.
12. Lindell, I. V., A. H. Sihvola, S. A. Tretyakov, and A. J. Viitanen, *Electromagnetic Waves in Chiral and Bi-isotropic Media*, Artech House, Boston, London, 1994.
13. Munk, B., *Frequency Selective Surfaces: Theory and Design*, John Wiley & Sons, New York, 2000.
14. Pozar, D. M., *Microwave Engineering*, John Wiley & Sons, New

York, 1998.

15. Rikte, S., G. Kristensson, and M. Andersson, "Propagation in bianisotropic mediareflection and transmission," *IEE Proc. Microwaves, Antennas and Propagation*, Vol. 148, No. 1, 29–36, 2001.
16. Shuley, N. V., "Analytical and numerical study of two-dimensional multilayer structures for use as dichroic surfaces," Technical Report TR 8404, Division of Network Theory, Chalmers University of Technology, 1984.
17. Wait, J. R., *Electromagnetic Waves in Stratified Media*, second edition, Pergamon, New York, 1970.

Gerhard Kristensson received the B.S. degree in mathematics and physics in 1973 and the Ph.D. degree in theoretical physics in 1979, both from the University of Gothenberg, Sweden. He held positions at the University of Gothenberg and the Royal Institute of Technology before being appointed Chair of Electromagnetic Theory at Lund Institute of Technology. He has held visiting positions at Ames Laboratory (Iowa State University) and at the University of Canterbury (New Zealand). His main research interests are in electromagnetic wave propagation in inhomogeneous media, with special emphasis on inverse scattering problems.

Sören Poulsen was born in Helsingborg, Sweden, in 1968. He received the M.Sc. degree in mathematics from the University of Växjö, Sweden, in 1995, and the Lic.Eng. degree in electrical engineering from the University of Lund, Sweden, in 2000. Since 1995 he has been employed at Chelton Applied Composites in Sweden, working on the design of low observable radomes, as well as dielectrical radomes. His research interests include frequency selective structures and the design of radomes.

Sten Rikte was born on August 3, 1959, in Lidingö, Sweden. In 1986 he became M.Sc. in Engineering Physics, Lund University, Lund Institute of Technology, Sweden. In 1995 he received a Ph.D. in Electromagnetic Theory at Lund Institute of Technology. In 2001, he was appointed to docent, the highest academic title in Sweden. Mathematics and electromagnetics, in particular time-domain methods, are among his many interests. At present he is employed at Kockums AB as an electromagnetic signature expert.